ADVANCES IN ATMOSPHERIC SCIENCES, VOL. 41, AUGUST 2024, 1483–1495

• **Original Paper** •

Arctic Sea Ice Variations in the First Half of the 20th Century: A New Reconstruction Based on Hydrometeorological Data※

Vladimir A. SEMENOV*[1,2], Tatiana A. ALDONINA[1,2], Fei LI[3], Noel Sebastian KEENLYSIDE*[3,4], and Lin WANG[5]

[1]*A.M. Obukhov Institute of Atmospheric Physics RAS*, *Moscow* 119017, *Russia*

[2]*Institute of Geography RAS*, *Moscow* 119017, *Russia*

[3]*Geophysical Institute*, *University of Bergen and Bjerknes Centre for Climate Research*, *Bergen* 5007, *Norway*

[4]*Nansen Environmental and Remote Sensing Center*, *Bergen* 5007, *Norway*

[5]*Center for Monsoon System Research*, *Institute of Atmospheric Physics*, *Chinese Academy of Sciences*, *Beijing* 100029, *China*

(Received 4 November 2023; revised 15 June 2024; accepted 21 June 2024)

ABSTRACT

The shrinking Arctic sea-ice area (SIA) in recent decades is a striking manifestation of the ongoing climate change. Variations of the Arctic sea ice have been continuously observed by satellites since 1979, relatively well monitored since the 1950s, but are highly uncertain in the earlier period due to a lack of observations. Several reconstructions of the historical gridded sea-ice concentration (SIC) data were recently presented based on synthesized regional sea-ice observations or by applying a hybrid model–empirical approach. Here, we present an SIC reconstruction for the period 1901–2019 based on established co-variability between SIC and surface air temperature, sea surface temperature, and sea level pressure patterns. The reconstructed sea-ice data for March and September are compared to the frequently used HadISST1.1 and SIBT1850 datasets. Our reconstruction shows a large decrease in SIA from the 1920 to 1940 concurrent with the Early 20th Century Warming event in the Arctic. Such a negative SIA anomaly is absent in HadISST1.1 data. The amplitude of the SIA anomaly reaches about 0.8 mln km^2 in March and 1.5 mln km^2 in September. The anomaly is about three times stronger than that in the SIBT1850 dataset. The larger decrease in SIA in September is largely due to the stronger SIC reduction in the western sector of the Arctic Ocean in the 70°–80°N latitudinal zone. Our reconstruction provides gridded monthly data that can be used as boundary conditions for atmospheric reanalyses and model experiments to study the Arctic climate for the first half of the 20th century.

Key words: Arctic sea ice, Arctic climate, early 20th century warming, climate variability

Citation: Semenov, V. A., T. A. Aldonina, F. Li, N. S. Keenlyside, and L. Wang, 2024: Arctic sea ice variations in the first half of the 20th century: A new reconstruction based on hydrometeorological data. *Adv. Atmos. Sci.*, **41**(8), 1483–1495, https://doi.org/10.1007/s00376-024-3320-x.

Article Highlights:

- A new gridded Arctic sea-ice reconstruction for 1901–2019 using co-variability between sea ice and hydrometeorological data is presented.
- The new reconstruction shows a large negative sea-ice anomaly in the middle of the 20th century comparable to the modern decline.
- The new reconstruction can be used as boundary conditions for atmospheric reanalyses and models for the first half of the 20th century.

1. Introduction

Global warming in recent decades has been accompanied by a rapid decline in the Arctic sea ice. Occurring during the era of continuous passive microwave satellite observations, this is probably the most well-monitored and impressive manifestation of the changing climate system (Cavalieri and Parkinson, 2012). Since 1979, the Arctic sea-ice area [SIA,

※ This paper is a contribution to the special topic on Ocean, Sea Ice and Northern Hemisphere Climate: In Remembrance of Professor Yongqi GAO's Key Contributions.

* Corresponding authors: Vladimir A. SEMENOV, Noel Sebastian KEENLYSIDE
Emails: vasemenov@ifaran.ru, noel.keenlyside@uib.no

area-integrated sea-ice concentration (SIC)] has been decreasing by about 11% per decade in September (Matveeva and Semenov, 2022). This rapid transformation of the cryosphere has important consequences for Arctic ecosystems, society, and economies (Meier et al., 2014). These impacts extend to the northern high latitudes (Bengtsson et al., 2004; Alexeev et al., 2017; Ivanov et al., 2018), midlatitude atmospheric circulation in the Northern Hemisphere (Gao et al., 2015), and global mean surface temperature (Semenov et al., 2010; Huang et al., 2017b).

The rapid acceleration of Arctic sea-ice melt during the first decade of the 21st century has raised concerns about a seasonally ice-free Arctic in the near future (Wang and Overland, 2012). It appears to be caused mainly by external forcing, as global climate models driven by historical forcing reproduce most of the decline in SIA (Semenov et al., 2015). These models indicate that September SIA may become lower than 1 mln.km^2 before 2050, following all currently adopted emission scenarios (Notz and SIMIP Community, 2020).

Past changes in Arctic sea ice are relevant for understanding the dynamics and magnitude of internal climate variability in sea ice and associated climatic trends, and thus for assessing climate models. Decadal to multidecadal variations in sea ice have been tracked back to the 16th century in some regions (Miles et al., 2014). Such variations have been linked to fluctuations in oceanic and atmospheric heat transport to the Arctic (Deser and Teng, 2008; Polyakov et al., 2017; Årthun et al., 2019), and further attributed to the Atlantic Multidecadal Oscillation (Day et al., 2012; Zhang, 2015) and Pacific Decadal Variability (Tokinaga et al., 2017; Svendsen et al., 2021). Understanding the magnitude and mechanisms of internal Arctic SIA variations is thus crucial for assessing future projections of the Arctic climate (Swart et al., 2015).

Of particular interest is the large-scale multidecadal warming of the Arctic that occurred during the Early 20th Century Warming (ETCW) and whose amplitude was only exceeded in the last two decades (Bokuchava and Semenov, 2021). Internal climate variability involving positive feedbacks in the Arctic was found to be a primary contributor to the ETCW (Bengtsson et al., 2004; Bokuchava and Semenov, 2020). However, our understanding of the ETCW of the Arctic is poor. Even whether an Arctic SIA reduction accompanied the ETCW is an open question.

Gaps in sea-ice observations are the main limitation to our understanding of the ETCW of the Arctic. Although surface air temperature (SAT) in the Arctic is relatively well documented during the ETCW (Kuzmina et al., 2008; Bekryaev et al., 2010), the sea-ice conditions for that period remain uncertain. While there are some observations of sea ice in the marginal Arctic seas in summertime (Polyakov et al., 2003), there are none in the inner Arctic Ocean. In wintertime, the situation with observations is much worse (Walsh et al., 2017): whereas the Russian Arctic seas exhibit a negative multidecadal anomaly in SIA during the ETCW (Zakharov, 1997; Polyakov et al., 2003; Johannessen et al., 2004), the Nordic seas show no such multidecadal variation (Vinje, 2001). Commonly used gridded datasets, such as HadISST1.1, provide mostly climatological SIC data prior to the 1950s, because of these data gaps (Rayner et al., 2003). This could compromise results from atmospheric general circulation model experiments, which do not reproduce the ETCW of the Arctic when forced by such gridded data (Semenov and Latif, 2012). Thus, although the link between SAT and sea ice implies that the ETCW was accompanied by a concurrent reduction in Arctic sea ice, the magnitude and extent of the decline are unclear.

A reliable reconstruction of SIC for the first half of the 20th century is required to address these uncertainties. The link between Arctic SAT and sea ice was recently used to produce a time series of SIA anomalies for the whole Arctic and its subregions (Alekseev et al., 2016; Connolly et al., 2017). The September sea-ice extent (SIE, integral sum of the areas of all grid cells with at least 15% SIC) reconstructed by Alekseev et al. (2016) showed a strong (about 1 mln.km^2) negative anomaly peaking in the 1930s. Walsh et al. (2017) produced the first comprehensive gridded monthly Arctic SIC reconstruction extending back to 1850 (SIBT1850), through combining available historical Arctic sea-ice data and analog-based estimations of SIC in areas with no data. In another approach, Brennan et al. (2020) performed ensemble Kalman filter data assimilation on SAT observations and Last Millennium climate model simulations to create a gridded reconstruction of annual Arctic SIC from 1850 to 2018. In the other approach, Semenov and Matveeva (2020) used a regression model based on the empirical orthogonal function (EOF) decomposition of SAT and SIC to reconstruct the monthly SIC for the period 1901–53; the regression model was based on the period with reliable SIC data (1953–2019). All three gridded datasets show a multidecadal negative SIA anomaly around the mid-20th century, but the anomaly is weakest in SIBT1850.

The aim of this study is to introduce another method to reconstruct SIC data that is based solely on observations. We use a similar approach to Semenov and Matveeva (2020), but, anong with SAT observations, SST and sea level pressure (SLP) data are additionally used, and individual regression models are constructed for three geographically separated regions. This considerably improves the fit of the regression models. The results of the new SIC reconstruction [hereafter referred to as IAPICE1 (Institute of Atmospheric Physics sea ICE reconstruction version 1)] are presented and compared to SIBT1850 and HadISST1.1 data.

2. Data and methods

We reconstruct the monthly Arctic SIC for the period 1901–2019 using observations of SAT over land areas, SST, and SLP. We use SST, SAT, and SLP data because of their physical relation to SIC variability and because they have much better temporal and spatial coverage and reliability during the earlier period than SIC data, which are severely limited regionally and seasonally prior to 1953.

Our method has three main steps. First, for each month, predictors' fields, including SAT, SST, and SLP, are decomposed into EOFs for the period 1901–2019, and predictand SIC fields are decomposed into EOFs for the period 1953–2019, when there are reliable SIC data. This reduces the dimensionality of the data and helps to identify spatio-temporal features of variations, thereby better revealing the underlying large-scale physical relations. Second, multiple linear regression models are built to explain predictand (SIC) principal components (PCs) variations by predictors' (SAT, SST, and SLP) PCs based on the period 1953–2019. A limited number of PCs that explain the major part (more than 90%) of the corresponding predictor and (more than 98%) of the predictand variability are used. Finally, the regression models are used to reconstruct SIC PCs for the period 1901–52 (except for the Sea of Okhotsk, where the regression models are built based on the period 1979–2019 and SIC PCs are reconstructed for 1901–1978) and restore SIC fields using corresponding EOFs. Although continuous satellite observations started in 1979, regular SIC observations from ships, aircrafts and drifting buoys of large geographical coverage provided a basis for the first gridded SIC dataset starting from 1953 (Walsh and Johnson, 1979). Notable differences in SIA variability from HadISST1.1 after and before 1953, when climatological SIC data have been used for some periods, are visible in Fig. 1. Sea-ice data coverage problems are discussed in detail in several studies (Walsh and Johnson, 1979; Rayner et al., 2003; Walsh et al., 2017; Matveeva and Semenov, 2022).

The reconstruction method used in this study extends on that of Semenov and Matveeva (2020) by including SST and SLP data as predictors (in addition to SAT); not using temporal filtering data (previously a 5-year running mean was applied to the PCs); and by constructing different regression models for the three geographically divided Arctic regions (instead of considering the Arctic as a whole): the Arctic Ocean (including the Atlantic Sector), Bering Sea, and Sea of Okhotsk (the sea masks are shown in Fig. S1, in the Electronic Supplementary Material, ESM). These three Arctic sub-regions represent different oceanic circulation systems that are affected largely by different forcing factors. A slightly different set of predictors is used for each region, as summarized below. This resulted in a considerably improved fit in the modern period and a more reliable reconstruction for the first half of the 20th century.

For the Arctic Ocean, without the Pacific sector, a regression model is built for the first six PCs of the EOF decomposition of SIC anomalies (six leading EOF modes explain more than 98% of SIC variability) for the region north of 40°N for the period 1953–2019 [using data from the HadISST1.1 archive (Rayner et al., 2003), 1° × 1° lat/lon resolution]. The set of predictors includes the first six PCs of the EOF decomposition of SAT anomalies over land [based on data from the CRU TS 4.05 archive (Harris et al., 2020), 0.5° × 0.5° lat/lon resolution] over the Northern Hemisphere north of 30°N; the first four PCs of the EOF anomalies of SST [based on data from the ERSST.v5 archive (Huang et al., 2017a), 2° × 2° lat/lon resolution] in the North Atlantic region (30°–75°N); and the first six temporal coefficients of the EOF anomalies of SST in the northern part of the Pacific Ocean (30°–66°N)—see these regions marked in Fig. S1. The choice of the predictors' regions was based on trials, expertise, and a compromise between complexity and efficiency. Since predictors based on PCs for extratropical SLP variability made a negligible contribution to the explained variance, they are not included in the regression model for the Arctic Ocean SIC. The number of predictors' PCs used in the regression model was chosen so that the corresponding EOFs explained more than 90% of the predictor's variability for each month.

For the reconstruction of SIC in the Bering Sea, a regression model is built for the first four SIC PCs, explaining

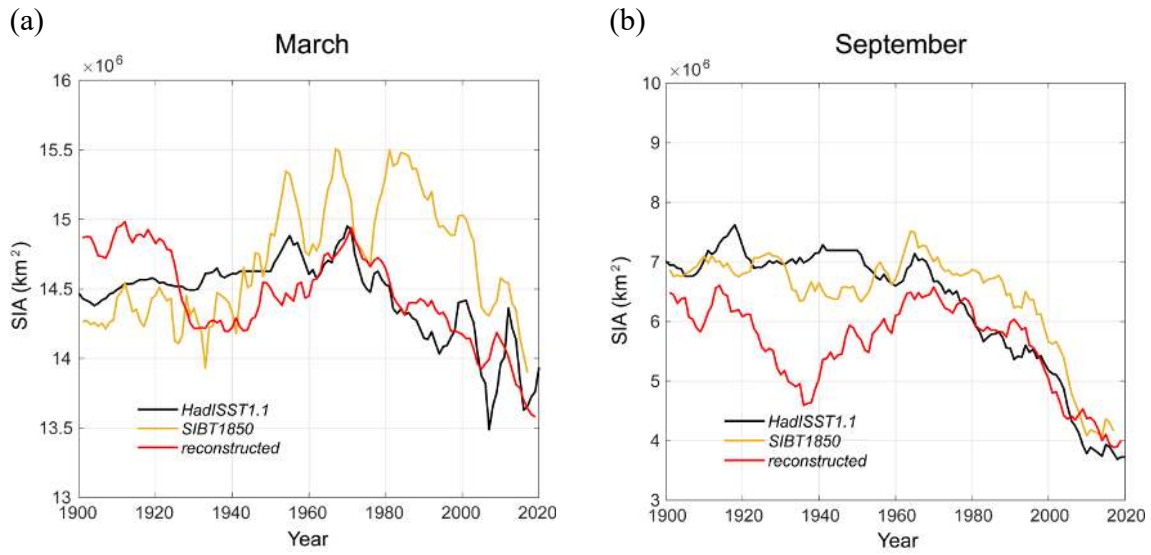

Fig. 1. Arctic SIA (units: km^2) in (a) March and (b) September according to HadISST1.1, SIBT1850, and the reconstructed data (IAPICE1). Data are smoothed with 5-yr running means.

more than 98% of the SIC variability for the period 1953–2019. The first four PCs of the SST EOF decomposition in the northern part of the Pacific Ocean (30°–66°N) and the first four PCs of the EOF decomposition of SLP [HadSLP2 archive (Allan and Ansell, 2006), 5° × 5° lat/lon resolution] in the region within 25°–75°N and 135°E–120°W (Fig. S1) were used as independent variables in the multiple regression model trained for the period 1953–2019. SAT PCs were not used as they contributed a very small portion of the explained variance.

The same set of predictors was used for the SIC in the Sea of Okhotsk as in the Bering Sea. However, the training period was restricted to 1979–2019 because the available SIC data in this sea are discontinuous at the end of the 1970s in the HadISST1.1 dataset, presumably due to introducing satellite data (Rayner et al., 2003). This discontinuity and other peculiarities of the evolution of SIA in the Sea of Okhotsk in the 20th century in different datasets are illustrated in Fig. S2 in the ESM.

For each sector, the three steps—decomposition, regression modeling, and reconstruction—are mathematically as follows: First, the monthly SIC anomaly (x, y, t) for 1953/79–2019 of the fairly reliable data (HadISST v1.1) is approximated by a sum of the K spatial patterns, $\mathrm{EOF}_i^{\mathrm{SIC}}(x, y)$, with corresponding PCs, $\mathrm{PC}_i^{\mathrm{SIC}}(t)$:

$$\mathrm{SIC}(x,y,t) = \sum_{i=1}^{N=K} \mathrm{PC}_i^{\mathrm{SIC}}(t)\,\mathrm{EOF}_i^{\mathrm{SIC}}(x,y)\,,$$

where x, y, and t are the latitude, longitude, and time, with 1° latitude, 1° longitude, and 1 month resolution, respectively; and $K = 6$ for the Arctic Ocean and 4 for the Bering Sea and Sea of Okhotsk. The SAT, SST, and SLP anomalies for 1901–2019 (relative to 1953/79–2019) are also approximated by a sum of EOFs as

$$\mathrm{SAT}(x,y,t) = \sum_{j=1}^{N=M1} \mathrm{PC}_j^{\mathrm{SAT}}(t)\,\mathrm{EOF}_j^{\mathrm{SAT}}(x,y)\,,$$

$$\mathrm{SST}(x,y,t) = \sum_{k=1}^{N=M2} \mathrm{PC}_k^{\mathrm{SST}}(t)\,\mathrm{EOF}_k^{\mathrm{SST}}(x,y)\,,$$

$$\mathrm{SLP}(x,y,t) = \sum_{l=1}^{N=M3} \mathrm{PC}_l^{\mathrm{SLP}}(t)\,\mathrm{EOF}_l^{\mathrm{SLP}}(x,y)\,,$$

where M1, M2, M3 are corresponding numbers of predictands' EOFs used for each of three sectors, see the description above.

Second, the least-squares method is used to calculate the multiple linear regression coefficients b_j^i, b_k^i, and b_l^i of $\mathrm{PC}_i^{\mathrm{SIC}}(t)$ with $\mathrm{PC}_j^{\mathrm{SAT}}(t)$, $\mathrm{PC}_k^{\mathrm{SST}}(t)$, and $\mathrm{PC}_l^{\mathrm{SLP}}(t)$, using data from 1953–2019 for the Arctic and Bering seas, and 1979–2019 for the Sea of Okhotsk:

$$\mathrm{PC}_{\mathrm{re}}^{\mathrm{SIC}}(i,t) = \sum_{j=1}^{N=M1} \mathrm{PC}_j^{\mathrm{SAT}} b_j^i + \sum_{k=1}^{N=M2} \mathrm{PC}_k^{\mathrm{SST}} b_k^i + \sum_{l=1}^{N=M3} \mathrm{PC}_l^{\mathrm{SLP}} b_l^i\,,$$

Third, the PCs are reconstructed for SIC $\mathrm{PC}_{\mathrm{re}}^{\mathrm{PC}}(t)$ using the regression model, and SIC (x, y, t) anomalies are reconstructed using the corresponding EOFs for the entire period of 1901–2019:

$$\mathrm{SIC}_{\mathrm{re}}(x,y,t) = \sum_{i=1}^{N=K} \mathrm{PC}_{\mathrm{re}}^{\mathrm{SIC}}(t)\,\mathrm{EOF}_i^{\mathrm{SIC}}(x,y)\,.$$

Then, the absolute SIC values are calculated using the relevant training period mean. If the reconstructed SIC values are negative or above 1, they are assigned 0 and 1, respectively. For the sake of generality, we leave all three predictors' sets (SAT, SST, and SLP) in the regression model and note again that different predictor sets were used for different regions, as described above. After recovering SIC data for three regions, the data are merged into a 1° × 1° archive with a monthly temporal resolution for the period 1901–2019. An example of the SIC PCs' variability explained by different predictors for March and September is given in Table S1.

We note that a linear regression model assumes a stationarity of the time series. This assumption may be questioned given a strong anthropogenic forcing and accelerated warming in the Arctic that may considerably modify mechanisms of heat exchange between the ocean, sea ice, and atmosphere (Polyakov et al., 2017; Ivanov et al., 2018). The results of the reconstruction also depend on the predictors' data quality in the early 20th century period, which is usually much worse than in the modern climate period used to train the regression model. These are, however, general limitations for all reconstructions of the past based on regression models. In order to capture the multidecadal signal in the variability of the sea ice and predictors' variables, in particular the North Atlantic SST and sub-Arctic SAT, it is important to train the regression model for a sufficiently long period, which should be at least as long as one cycle (but preferably more) of the dominant multidecadal variations (60–70 years). This compels us to use all reliable data periods of 1953–2019 to train the regression model.

The reconstructed SIC data (IAPICE1) are compared to the most frequently used data from HadISST1.1 (Rayner et al., 2003) and another reconstruction, SIBT1850, based on the compilation of empirical data using interpolation and an analog-based approach for filling gaps (Walsh et al., 2017). The data are compared for the entire Arctic and different Arctic seas, which are defined according to the recommendations of the International Hydrographic Organization.

3. Results

The Arctic SIA for March and September (months of maximum and minimum SIE in the Northern Hemisphere) based on IAPICE1, and from the HadISST1.1 and

SIBT1850 archives, are compared (Fig. 1). For March, there are substantial discrepancies among the different datasets, even for the modern period (Fig. 1a). In some years, the SIA calculated from SIBT1850 data exceeds that of HadISST1.1 and IAPICE1 by 1 mln.km^2, and the pronounced maximum in SIBT1850 in the early 1980s is absent in IAPICE1 and HadISST1.1 data. It is worth noting that the relatively good agreement between the HadISST1.1 and IAPICE1 data for the modern period indicates the success of the reconstruction methodology (and goodness of fit of the regression model). In the first half of the 20th century, SIA experienced no significant decadal variations or trends according to the HadISST1.1 data. However, both the SIBT1850 and our reconstruction, IAPICE1, show a long-term negative anomaly. The minimum extent according to SIBT1850 occurs in the mid-1930s, while in IAPICE1 it spans the 1930s to the 1940s. Relative to the SIA in the first two decades of the 20th century, the maximum negative anomaly corresponds to approximately 0.4 and 0.7 mln.km^2, based on the SIBT1850 and IAPICE1 data, respectively. This is due to the much larger SIA at the beginning of the 20th century (by about 0.5 mln.km^2) in IAPICE1 compared to SIBT1850. This feature results in a distinct multidecadal negative SIA anomaly in our reconstruction that is absent in the SIBT1850 and HadISST1.1 data.

For September, the evolution of the SIA from the second half of the 20th century shows better consistency in all three archives (Fig. 1b). However, the SIBT1850 SIA is on average larger by 0.6 mln.km^2 compared with the HadISST1.1 and IAPICE1 data from the beginning of the 1960s to the early 2000s. The SIA in the first half of the 20th century, according to HadISST1.1 data, demonstrates relatively weak decadal fluctuations without pronounced trends. In the early 1940s, the HadISST1.1 data represent constant values due to filling of data gaps during and after World War 2. According to SIBT1850 and IAPICE1, there is a negative SIA anomaly in the 1930s–40s, with a much larger anomaly in IAPICE1. The anomaly magnitude at the end of the 1930s, compared to the values at the beginning of the 20th century, was approximately 1.5 mln.km^2, according to IAPICE1, and about 0.6 mln.km^2 according to SIBT1850. In IAPICE1, the SIA anomaly in the 1930s–40s is comparable to the SIA anomaly at the end of the 20th century.

The most noticeable differences in the Arctic SIE among IAPICE1, HadISST1.1, and SIBT1850 during the mid-20th century minimum in 1935–45 are found in September (Fig. 2). In the HadISST1.1 data, the SIE is much larger than in SIBT1850 and IAPICE1 data, covering the central Arctic and all marginal seas along the eastern and westerns coasts except the Barents Sea (Fig. 2a). This disagrees with the available summer observations for the Russian Arctic seas that show a significant SIE decrease in the 1940s in late summer (Polyakov et al., 2003). Such a decrease is present in both SIBT1850 and IAPICE1 with large areas of open water in the Russian Arctic seas east to Novaya Zemlya, in the Chukchi and Beaufort seas in the western Arctic. Compared to SIBT1850, IAPICE1 data exhibit a stronger retreat of sea ice in the East Siberian and Chukchi seas and along the East Canadian Coast, also with some open water areas in the Canadian Archipelago. SIBT1850, however, shows less sea ice in the eastern part of the Kara Sea.

The spatial structure of the rate of change of SICs according to HadISST1.1, SIBT1850, and IAPICE1 archives during the ETCW period (1915–45) differs significantly. Since the main SIC changes in March occurred in the Atlantic and Pacific sectors of the Arctic, SIC trends are presented separately for each of these sectors for a more detailed analysis (Fig. 3). In the Atlantic sector, according to HadISST1.1 data (Fig. 3a), there are almost no SIC changes for the period 1915–45. SIBT1850 data (Fig. 3b) exhibit some noticeable areas of negative trends accompanied by some spots with positive trends around the marginal sea-ice zone. The rates of change are not high, at up to 5%–7% (10 yr)$^{-1}$, both for decreasing and increasing SIE. In contrast, the IAPICE1 data (Fig. 3e), show large areas with strongly decreasing SIC trends in the eastern and southern part of the Barents Sea, where SIC trends exceed −25% (10

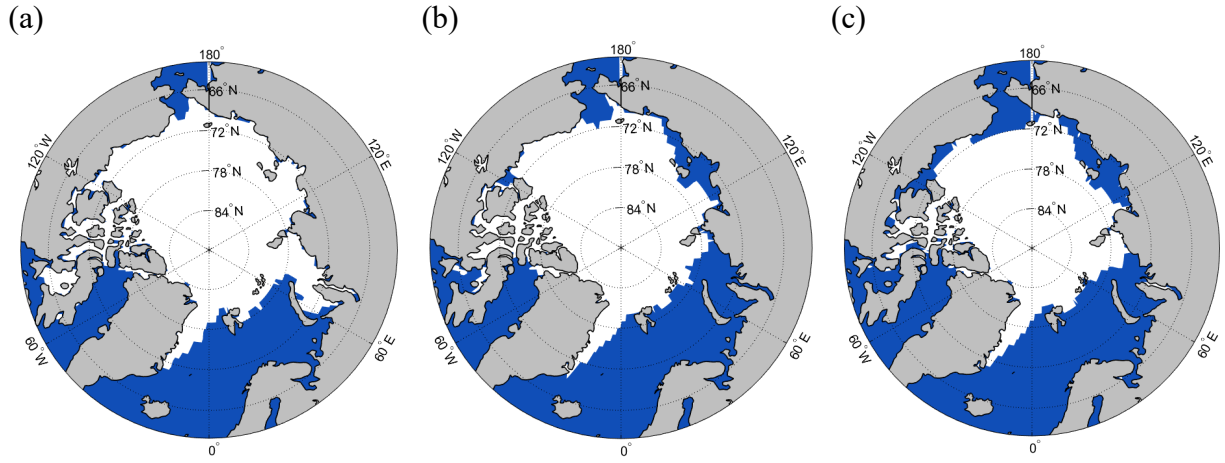

Fig. 2. September Arctic SIE averaged for the period 1935–45 according to (a) HadISST1.1, (b) SIBT1850, and (c) IAPICE1.

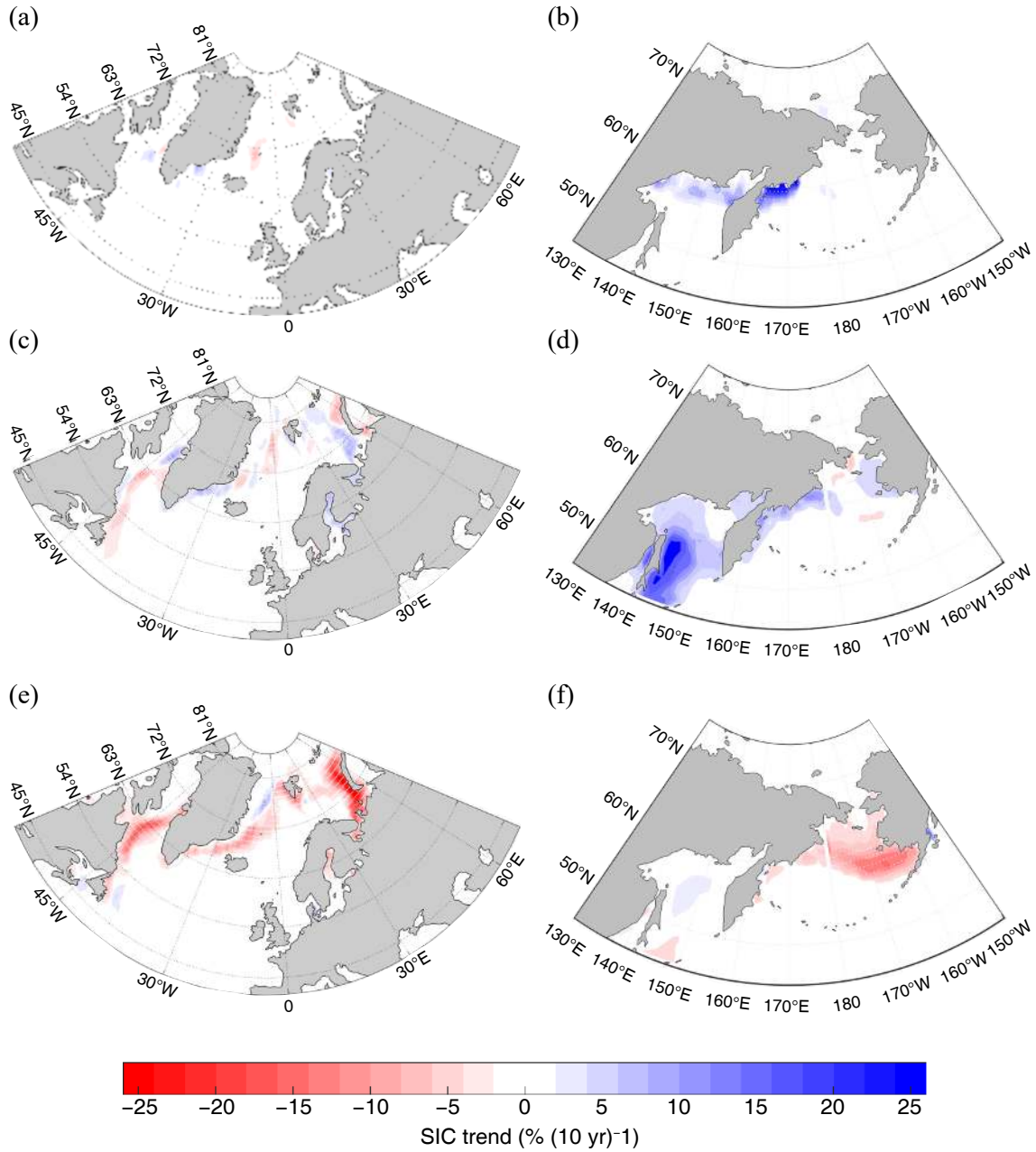

Fig. 3. March SIC trends [units: % (10 yr)$^{-1}$] in the (a, c, e) Atlantic and (b, d, f) Pacific sectors for the period 1915–45 according to (a, b) HadISST1.1, (c, d) SIBT1850, and (e, f) IAPICE1 data. White dots indicate trends significant at the 90% confidence level.

yr)$^{-1}$. Available observations indicate negative trends of the winter SIA in the Barents Sea in the first half of the 20th century (Krasheninnikova and Krasheninnikova, 2019; Timokhov et al., 2019). Noticeably decreasing SIC trends are seen in the Greenland Sea, the southern part of Baffin Bay, and the Labrador Sea, where SIC trends reach −15% to −20% (10 yr)$^{-1}$.

In the Pacific sector, March SIC trends for 1915–45 vary significantly between the HadISST1.1, SIBT1850, and IAPICE1 archives, to the extent of having opposite directions of SIC changes in some regions (Figs. 3b, d, and f). According to HadISST1.1 (Fig. 3b), SIC increased in the western part of the Bering Sea [with trends reaching up to 20% (10 yr)$^{-1}$], as well as in the northern part of the Sea of Okhotsk [with change rates of around 10%–12% (10 yr)$^{-1}$]. According to SIBT1850 (Fig. 3d), the SIC also predominantly increased in the Pacific sector, with vast areas of positive trends in the southern part of the Sea of Okhotsk and to the east of Sakhalin Island, where the rates of change exceeded 20% (10 yr)$^{-1}$. There is also a slight SIC increase [5%–7% (10 yr)$^{-1}$] in the coastal regions of the western and eastern parts of the Bering Sea. The reconstructed data (Fig. 3f), in contrast to both HadISST1.1 and SIBT1850, show a large area of negative trends in the eastern part of the Bering Sea,

where the SIC decreases by 10%–12% (10 yr)$^{-1}$. In the Sea of Okhotsk, slight regional trends [less than 2% (10 yr)$^{-1}$] of opposite signs are found. Such opposite SIC trends are consistent with the March SST and SAT changes for the corresponding period. There is a negative temperature trend in the northern part of the Bering Sea and adjacent land areas, and a positive trend in the Sea of Okhotsk and over the Kamchatka Peninsula (Fig. S3 in the ESM).

In terms of the wintertime sea-ice trends, SIBT1850 and IAPICE1 are in qualitative agreement in the Atlantic sector, but there is a substantial disagreement between the datasets in the Pacific sector. SIBT1850 shows an increase of SIC in the southwestern part of the Sea of Okhotsk, whereas IAPICE1 data exhibit a decrease in the northeastern part of the Bering Sea. It is difficult to assess the real picture during this period in wintertime. According to in situ observations of SIE in the Sea of Okhotsk (Pishchalnik et al., 2016), the period from the 1920s to the 1950s was characterized by a negative SIE trend. Such a trend is absent in HadISST1.1, SIBT1850, or IAPICE1 data. On the contrary, based on the first two datasets, significant SIC growth is noted for the period 1915–45. However, in situ SIE observations and gridded data from the analyzed archives are not directly comparable, and such a disagreement requires further assessment. Whereas some observations on the sea-ice conditions in the Sea of Okhotsk are available from the late 19th century, observations on the wintertime sea ice in the Bering Sea are available in the literature only from the beginning of the 1950s (Plotnikov and Vakulskaya, 2012). Furthermore, an analysis of different types of observations from the 1960s (Vakulskaya et al., 2014) indicates anti-phase SIE variations in the Bering and Okhotsk seas. This feature is qualitatively found in the IAPICE1 data (Fig. 3f).

In September, the major SIC changes in the first half of the 20th century happen not only around seasonal marginal zones, as in wintertime, but also in the inner Arctic Ocean. The Pacific sector is ice-free in September. According to HadISST1.1 data (Fig. 4a), the maximum negative SIC trends for the period 1915–45 are observed in Baffin Bay [exceeding −17% (10 yr)$^{-1}$]. SIC reduction is noted in the northern parts of the Barents and Kara seas [reaching −10% (10 yr)$^{-1}$], and in the East Siberian and Laptev seas [reaching −7% (10 yr)$^{-1}$]. At the same time, HadISST1.1 shows an SIC increase along the continental coastline [positive trends up to 10%–12% (10 yr)$^{-1}$] in the Kara, East Siberian, Chukchi, and Beaufort seas. SIBT1850 data (Fig. 4b) exhibit quite a different pattern of SIC trends. The highest rates of decline are found in the seas of the Russian part of the Arctic, particularly in the eastern part of the Kara Sea in the north and northeast of the Laptev Sea, the East Siberian Sea, and in the central part of the Chukchi Sea. Similar to HadISST1.1, SIBT1850 shows negative but weaker trends in Baffin Bay and around the Canadian Archipelago. However, in contrast to HadISST1.1, positive SIC trends are observed to the north of the Barents Sea. According to IAPICE1 data (Fig. 4c), SIC changes are negative everywhere in the Arctic during the period 1915–45. The areas of SIC reduction are more extensive. Along with the vast areas of negative trends in the seas of the Russian Arctic, which are also found in SIBT1850 data, there are large areas of SIC decline in the western part of the Arctic Ocean, which are absent in either the HadISST1.1 or SIBT1850 datasets. In contrast to those datasets, IAPICE1 data also show an SIC decrease north of 80°N. Negative trends in the Greenland and Barents seas are also stronger and cover larger areas.

Let us next take a closer look at the sea-ice changes in different Arctic seas over the course of the 20th century. The ETCW had different impacts on SIA variations in different seas. Since some seas are ice-free in September, while others are usually almost entirely covered by sea ice in March, we present the evolution of SIA for the seas in either March or September, depending on which season SIA exhibits large variability. For example, in the Barents Sea, there was a significant negative wintertime SIA anomaly observed from the 1930s to the 1950s, which is confirmed by other research findings (e.g., Krasheninnikova and Krasheninnikova, 2019; Timokhov et al., 2019). However, according to HadISST1.1, there is a "plateau" until 1953 due to the absence of reliable data (Fig. 5a). SIBT1850 data show a negative anomaly of SIA in the Barents Sea in the mid-20th century, but it is not as large as inferred from IAPICE1 data. The SIA reduction in IAPICE1 data from the beginning of the 20th century to the 1940s amounts to about 150 × 10^3 km^2, whereas the corresponding SIA change in SIBT1850 is about three times smaller; this is also due to lower SIA in the 1900s and 1910s in SIBT1850 than in our reconstruction. The reconstructed SIA in the Barents Sea in the mid-20th century is comparable to values in the early 2000s. The SIA maxima in the late 1960s and 1970s are found in all three datasets. The presence of these maxima is also confirmed by the results of other studies (e.g., Årthun et al., 2012).

In the Bering Sea (Fig. 5b), the March SIA exhibits decadal variations in all analyzed datasets from the 1950s. HadISST1.1 and SIBT1850 show no decadal variability until 1953, whereas IAPICE1 data exhibit an SIA increase around the 1920s followed by a decrease in the 1940s. Such decadal variations are likely associated with the Pacific Decadal Oscillation (PDO), which has a significant impact on the dynamics of sea ice in the Bering Sea (Zhang et al., 2010; Wendler and Wong, 2019; Yang et al., 2020). The variations in the PDO and SIA in the Bering Sea are in antiphase, as the negative PDO phase is associated with negative SST anomalies in the northern part of the Pacific Ocean. This leads to a weakening of the Aleutian low, resulting in a decrease of the warm air advection from the south into the Bering Sea, favoring an increase in SIA (Wendler et al., 2014).

In Baffin Bay, the March SIA in all datasets does not show a secular trend over the analyzed period (Fig. 5c). Instead, it exhibits decadal fluctuations starting from the 1950s, which are almost identical in the HadISST1.1 and

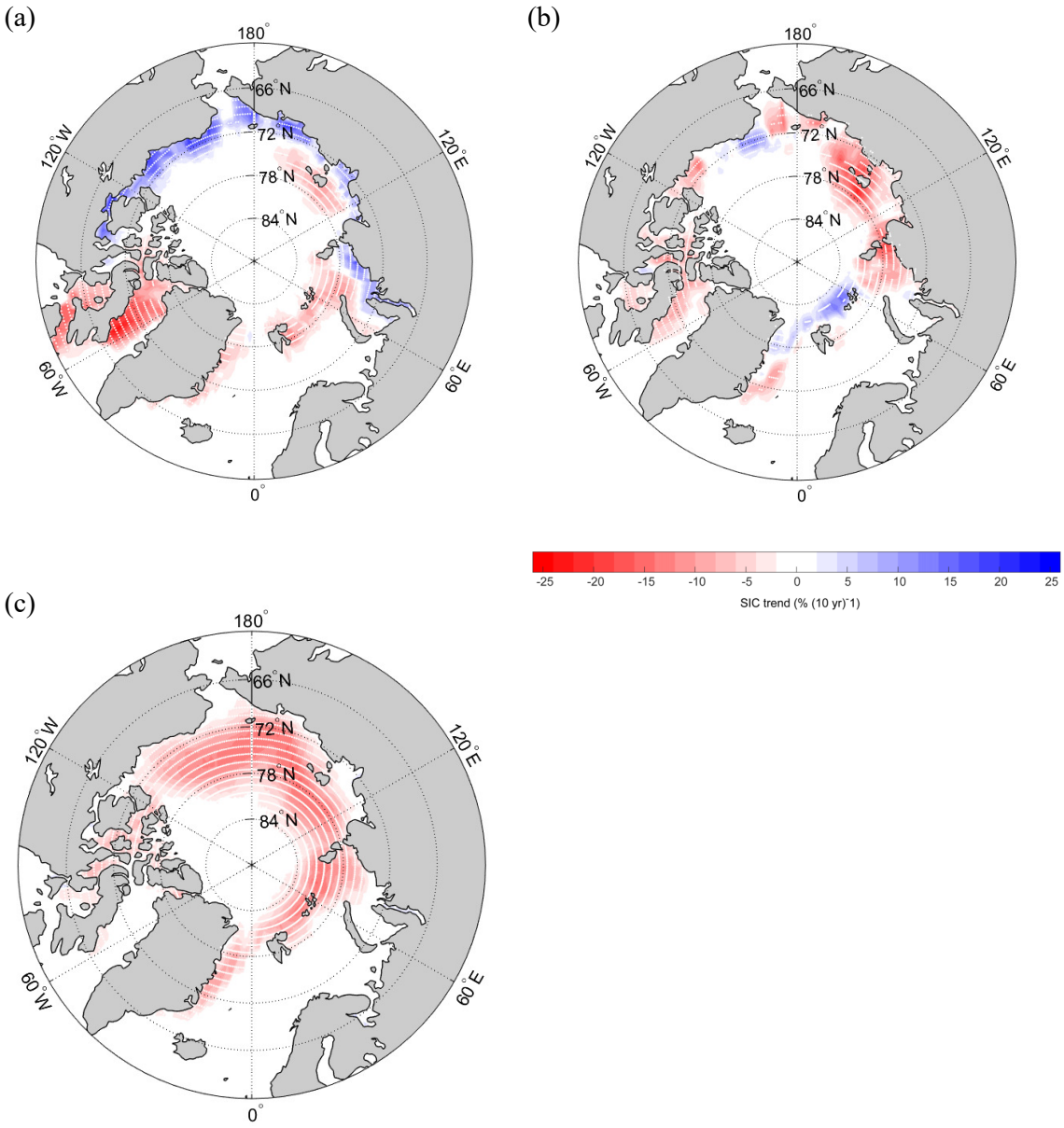

Fig. 4. September SIC trends [units: % (10 yr)$^{-1}$] for the period 1915–45 according to (a) HadISST1.1, (b) SIBT1850, and (c) IAPICE1 data. White dots indicate trends significant at the 90% confidence level.

IAPICE1 data, and well correlated with the SIBT1850 data, which have systematically higher SIAs. In the first half of the 20th century, the March SIA in SIBT1850 and HadISST1.1 has no significant decadal variations, whereas IAPICE1 reveals a negative SIA anomaly in the Baffin Sea during the 1930s–50s.

In the Greenland Sea (Fig. 5d), during the second half of the 20th century, IAPICE1 and HadISST1.1 data for the March SIA show good agreement. However, IAPICE1 underestimates the SIA peak in the late 1960s, while SIBT1850 fully agrees with HadISST1.1 during this peak. However, for the rest of the period from the mid-20th century, SIBT1850 significantly overestimates SIA values. This SIA peak is apparently associated with the formation of the Great Salinity Anomaly in the late 1960s in the northern part of the Atlantic Ocean. During this time, there was a decrease in surface-layer salinity, which resulted in a significant slowdown in ocean heat transport and local cooling. This favored an increase in the sea-ice cover in the Greenland Sea. The IAPICE1 and SIBT1850 data agree on a slight decrease in SIA in the 1940s that is absent in the HadISST1.1 archive.

In September, the largest SIA changes occur in the seas of the Russian sector of the Arctic, the northwest passages of the Canadian Archipelago, and in the central Arctic (Fig. 6). In general, SIA variations in all analyzed datasets agree relatively well after the 1960s. SIBT1850 data usually show systematically higher SIA values, whereas IAPICE1 data exhibit less decadal and sub-decadal SIA variations. The reconstructed SIA shows a multidecadal negative SIA

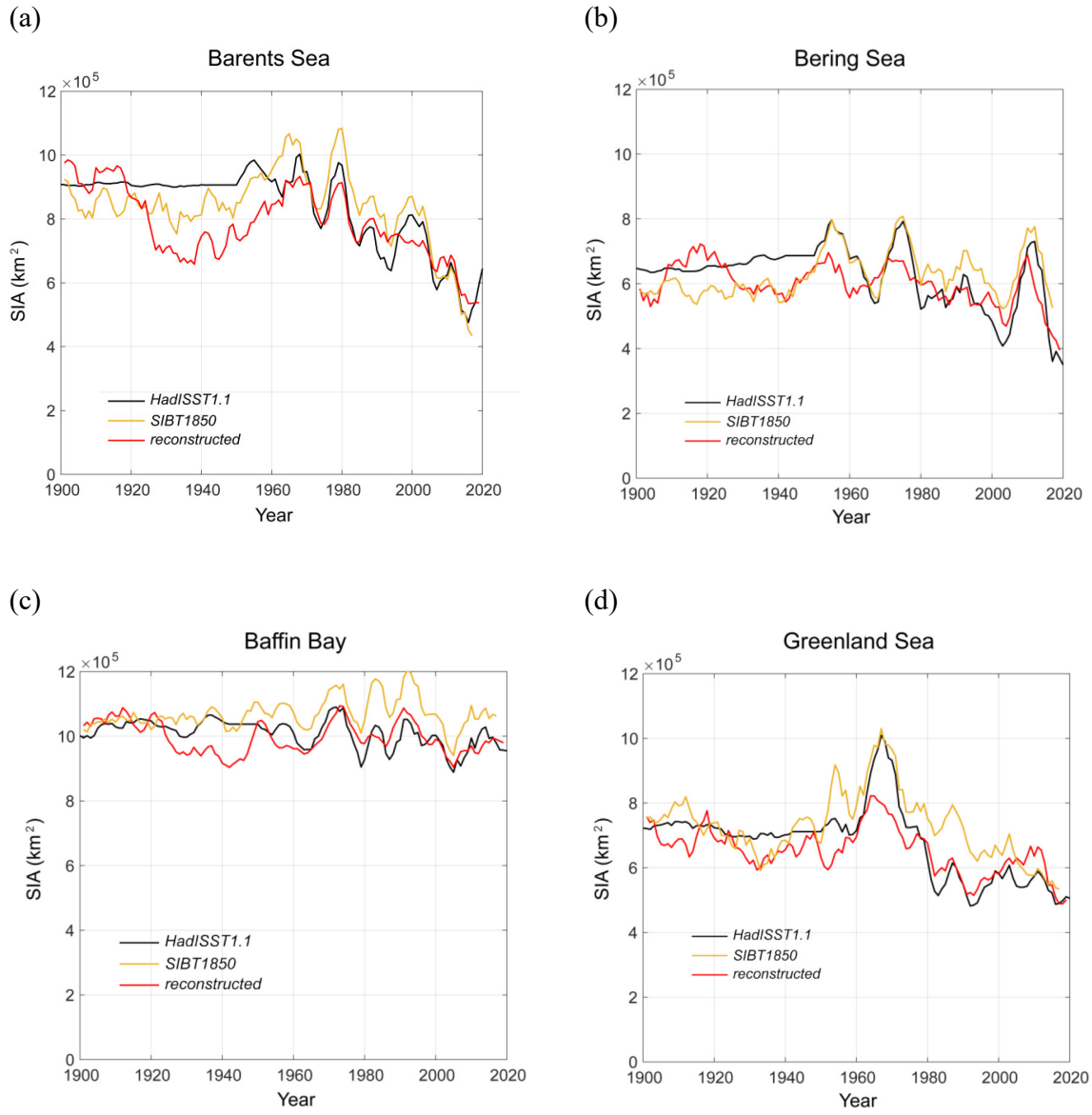

Fig. 5. March SIA (units: km^2) according to HadISST1.1, SIBT1850, and IAPICE1 data in the (a) Barents, (b) Bering, (c) Baffin, and (d) Greenland seas. Data are smoothed with 5-yr running means.

anomaly in the middle of the 20th century for all seas presented in Fig. 6. This reduction in SIE in the Russian Arctic during the summer period in the 1940s–50s is confirmed by the data from the Arctic and Antarctic Research Institute, Russia (Polyakov et al., 2003). The SIBT1850 dataset depicts a very similar negative SIA anomaly in the Kara Sea (Fig. 6a), and, to a lesser extent, in the East Siberian (Fig. 6b) and Laptev (Fig. 6c) seas, but it is absent in the northwest passages of the Canadian Arctic Archipelago (Fig. 6d), Beaufort Sea (Fig. 6e), and central Arctic (Fig. 6f) in SIBT1850. HadISST1.1 data do not show a corresponding multidecadal SIA anomaly, but exhibit negative decadal SIA fluctuations in the 1930s in the Kara, Laptev, and East Siberian seas.

The multidecadal SIA variability in the IAPICE1 dataset is associated with the first leading SIC EOF (Fig. S5 in the ESM). This EOF explains 45% to 65% of the total SIA variability for different months and is characterized by single-sign SIC anomalies in the Barents and Greenland seas in winter, and in the eastern and part of the central Arctic in summer, respectively (Fig. S6). In the regression model, the first SIC EOF is most closely linked to the first leading SST EOF in the North Atlantic (Table S1), which suggests a role of Atlantic multidecadal variability (Semenov et al., 2010; Miles et al., 2014).

We note that, when comparing different sea-ice data prior to 1979, the era of continuous satellite observations, no data can be considered as a benchmark to assess the quality of other data. Even for the satellite era, differences in retrieval algorithms may lead to systematic errors in the total Arctic SIE up to 1.3 mln.km^2 (Ivanova et al., 2014). There are also data for the August SIE in the Sea of the Eastern Arctic from Russian observations and analyses (Polyakov

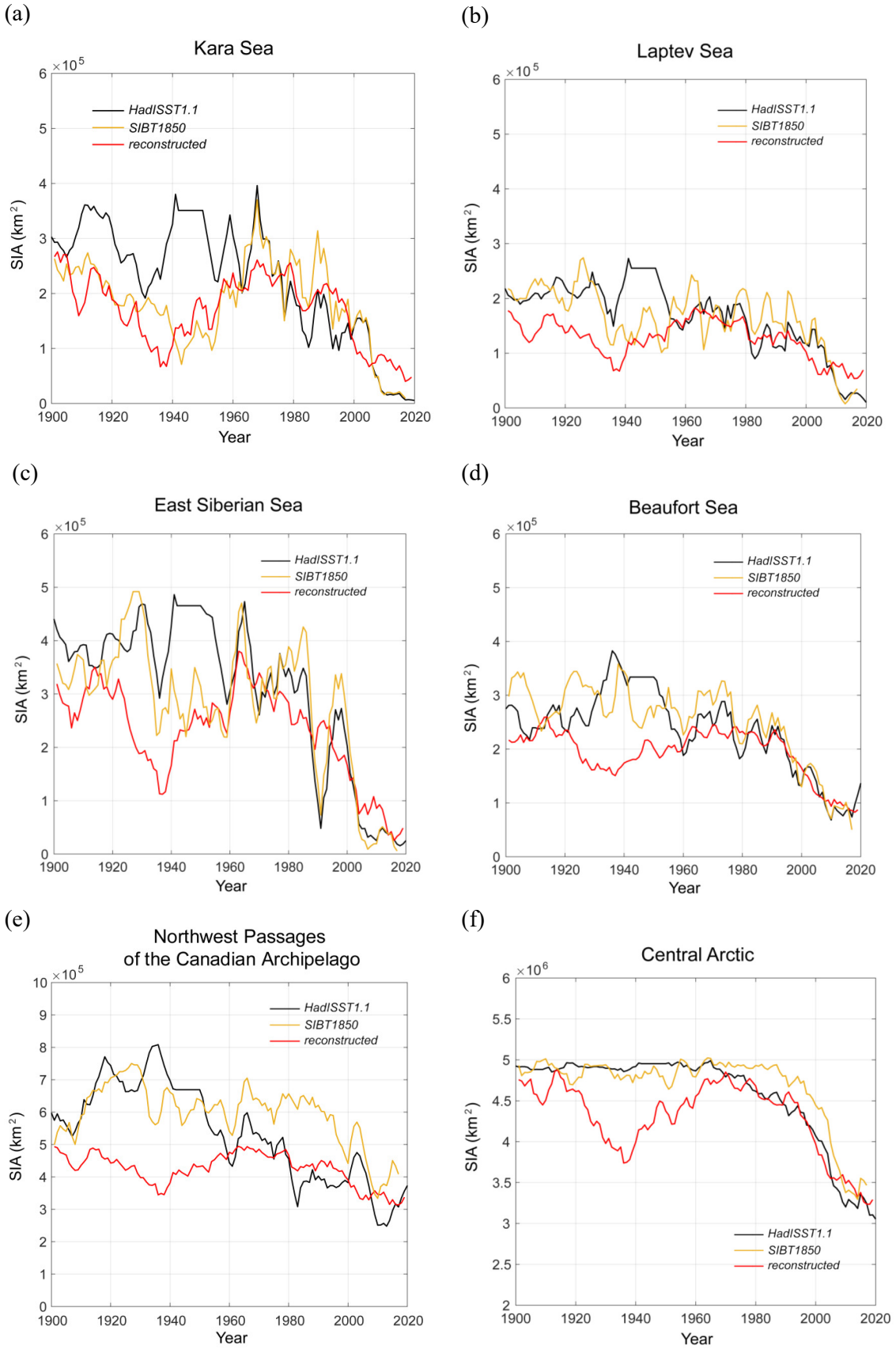

Fig. 6. September SIA (units: km^2) according to HadISST1.1, SIBT1850, and IAPICE1 data in the (a) Kara Sea, (b) Laptev Sea, (c) East Siberian Sea, (d) Beaufort Sea, (e) northwest passages of the Canadian Archipelago, and (f) central Arctic. Data are smoothed with 5-yr running means.

et al., 2003) extending back to 1900. A comparison of these data with the analyzed datasets (Fig. S4 in the ESM) shows that they are closer to the SIBT1850 data, but all datasets exhibit large differences in the SIE of the marginal seas before 1960s.

4. Summary and conclusions

A new 1° × 1° gridded dataset (IAPICE1) of monthly Arctic SIC for the period 1901–2019 is presented. The data are produced using a decomposition of monthly SIC (from HadISST1.1), SAT (CRU TS 4.05), SST (ERSST V5), and SLP (HadSLP2) fields into EOFs and building multiple regression models for SIC PCs. Regression models are constructed for the geographically separated regions of the Arctic Ocean, Bering Sea, and the Sea of Okhotsk using SAT, SST, and SLP PCs as predictors. The models are trained for periods with reliable data: 1953–2019 for the first two regions and 1979–2019 for the third. The SIC fields were reconstructed using this regression model from 1901.

The reconstructed sea-ice data for March and September were compared to the HadISST1.1 and SIBT1850 datasets. Both the SIBT1850 and IAPICE1 data exhibit a long-term negative Arctic SIA anomaly in March and September in the middle of the 20th century. The amplitude of the negative SIA anomaly in our reconstruction is about three times larger than in the SIBT1850 dataset and amounts to about 1.5 mln.km^2, with the SIA reduction reaching 4.5 mln.km^2 in the 1940s. In September, according to IAPICE1, the Arctic SIA in the 1930s–40s is comparable to the values in the late 20th century. The HadISST1.1 data exhibit no significant negative anomaly in Arctic SIA in this period.

The spatial structure of SIC trends in the Arctic for the period 1915–45 was intercompared for March in the Atlantic and Pacific sectors of the Arctic (where most robust SIC variations are observed in the winter) and for September in the entire Arctic. In the Atlantic sector in March, HadISST1.1 data exhibit no significant SIC changes, and SIBT1850 data show some modest SIC decreases in regions around the seasonal sea-ice marginal zone. In contrast, IAPICE1 demonstrates a substantial SIC reduction in the Labrador, Greenland, and Barents seas, with SIC trends reaching −25% (10 yr)$^{-1}$. In the Pacific sector, HadISST1.1 and SIBT1850 show a predominant SIC increase in the western part of the North Pacific in 1915–45, while in contrast, IAPICE1 data reveal a vast area of SIC decline in the eastern part of the Bering Sea. In September, IAPICE1 shows much larger areas of SIC decline compared to HadISST1.1 and SIBT1850, which spread into the inner Arctic Ocean north of 80°N, especially in the Canadian sector.

In the Arctic seas, which are not fully covered by sea ice in March or ice-free in September, the reconstructed SIA exhibits a multidecadal negative anomaly in the 1920s–40s in both seasons that is absent in HadISST1.1 data. For the first half of the 20th century, SIBT1850 data show similar SIA variations to the reconstructed data in the Greenland Sea in March, and in the Kara and Laptev seas in September. There is a strong disagreement between these datasets in the Beaufort Sea, northwest passages of the Canadian Archipelago, and central Arctic, where SIBT1850 does not exhibit a negative multidecadal anomaly in the 1920s–40s.

The IAPICE1 data show good agreement with the HadISST1.1 data starting from the 1960s, supporting our methodology. For the ETCW period, our reconstruction shows a much stronger negative SIA anomaly both in March and September than in SIBT1850, and is comparable to estimates from Brennan et al. (2020). We note, however, that Brennan et al. (2020) used a hybrid approach with data assimilation in a coupled climate model, whereas IAPICE1 is based on a statistical model using empirical data. In a qualitative agreement with other reconstructions (Alekseev et al., 2016; Walsh et al., 2017; Brennan et al., 2020), our results indicate that ETCW was accompanied by a strong concurrent negative SIA anomaly in the Arctic that was only exceeded by the modern SIA decline in the early 2000s. Thus, IAPICE1 data provide a new baseline for assessing internal climate variability. Nevertheless, the ongoing SIA decline is already significantly beyond the level of internal climate variability, even assuming that the ETCW of the Arctic was primarily caused by internal climate variations (Bokuchava and Semenov, 2020). This indicates the importance of the anthropogenic forcing.

Reconstructing past climate is a challenge, and our method, as with others, has caveats. As discussed in section 2, our approach relies on sampling the well-documented multidecadal variability in the Arctic SAT (e.g., Yamanouchi, 2011; Bokuchava and Semenov, 2021). This requires using the longest possible high-quality data to capture the relevant EOF patterns and regression relations. Thus, it is not possible to validate our approach using reliable independent data. Instead, we compare our data with another gridded reconstruction (Walsh et al., 2017) and an observational dataset, HadISST1.1 (Rayner et al., 2003), as well as with reanalyses and regional data available for some seasons and periods (see section 3 and Figs. S2 and S4). In general, we find a good agreement during the second half of the 20th century, and a qualitative agreement in the earlier period, with a stronger negative SIA anomaly during the ETCW. We hope this will motivate further studies to understand this key climate anomaly.

Our reconstruction provides a gridded monthly dataset for the first half of the 20th century and can be used, along with other gridded reconstructions, to study climate variability. For example, it can be used as the boundary condition for atmospheric GCM simulations to study the ETCW of the Arctic. At the same time, such simulations can also be used to evaluate the sea-ice data indirectly by comparison to available sub-Arctic observations of temperature and other climate variables (Semenov and Latif, 2012; Semenov, 2014). IAPICE1 data can also be used as boundary conditions in 20th century reanalyses that do not reproduce the ETCW in the Arctic correctly (Bokuchava and Semenov, 2021),

likely, in particular, due to erroneous sea-ice data.

Data availability. The IAPICE1 dataset is available at http://www.ifaran.ru/DATA/IAPICE1/, https://doi.org/10.11582/2024.00112, and https://doi.org/10.57760/sciencedb.iap.00005.

Acknowledgements. We would like to thank the three anonymous reviewers and the Editor for their valuable comments. The study was partly supported by the Russian Ministry of Science and Higher Education (Agreement No. 075-15-2021-577) and the Russian Science Foundation (Grant No. 23-47-00104). F. L. was funded by the Research Council of Norway (Grant No. Combined 328935). NK acknowledges the support of the Bjerknes Climate Prediction Unit with funding from the Trond Mohn Foundation (Grant No. BFS2018TMT01). LW acknowledges the support of the National Natural Science Foundation of China (Grant No. 42261134532).

Funding Note Open Access funding provided by University of Bergen (incl Haukeland University Hospital) .

REFERENCES

Alekseev, G., N. Glok, and A. Smirnov, 2016: On assessment of the relationship between changes of sea ice extent and climate in the Arctic. *International Journal of Climatology*, **36**, 3407–3412, https://doi.org/10.1002/joc.4550.

Alexeev, V. A., J. E. Walsh, V. V. Ivanov, V. A. Semenov, and A. V. Smirnov, 2017: Warming in the Nordic Seas, North Atlantic storms and thinning Arctic sea ice. *Environmental Research Letters*, **12**, 084011, https://doi.org/10.1088/1748-9326/aa7a1d.

Allan, R., and T. Ansell, 2006: A new globally complete monthly historical gridded mean sea level pressure dataset (HadSLP2): 1850–2004. *J. Climate*, **19**, 5816–5842, https://doi.org/10.1175/JCLI3937.1.

Årthun, M., T. Eldevik, and L. H. Smedsrud, 2019: The role of Atlantic heat transport in future arctic winter sea ice loss. *J. Climate*, **32**, 3327–3341, https://doi.org/10.1175/JCLI-D-18-0750.1.

Årthun, M., T. Eldevik, L. H. Smedsrud, Ø. Skagseth, and R. B. Ingvaldsen, 2012: Quantifying the influence of Atlantic heat on Barents sea ice variability and retreat. *J. Climate*, **25**, 4736–4743, https://doi.org/10.1175/JCLI-D-11-00466.1.

Bekryaev, R. V., I. V. Polyakov, and V. A. Alexeev, 2010: Role of polar amplification in long-term surface air temperature variations and modern Arctic warming. *J. Climate*, **23**, 3888–3906, https://doi.org/10.1175/2010JCLI3297.1.

Bengtsson, L., V. A. Semenov, and O. M. Johannessen, 2004: The early twentieth-century warming in the Arctic - A possible mechanism. *J. Climate*, **17**, 4045–4057, https://doi.org/10.1175/1520-0442(2004)017<4045:TETWIT>2.0.CO;2.

Bokuchava, D. D., and V. A. Semenov, 2020: Factors of natural climate variability contributing to the Early 20th Century Warming in the Arctic. *IOP Conference Series: Earth and Environmental Science*, **606**, 012008, https://doi.org/10.1088/1755-1315/606/1/012008.

Bokuchava, D. D., and V. A. Semenov, 2021: Mechanisms of the Early 20th Century Warming in the Arctic. *Earth-Science Reviews*, **222**, 103820, https://doi.org/10.1016/j.earscirev.2021.103820.

Brennan, M. K., G. J. Hakim, and E. Blanchard-Wrigglesworth, 2020: Arctic sea-ice variability during the instrumental era. *Geophys. Res. Lett.*, **47**, e2019GL086843, https://doi.org/10.1029/2019GL086843.

Cavalieri, D. J., and C. L. Parkinson, 2012: Arctic sea ice variability and trends, 1979–2010. *The Cryosphere*, **6**, 881–889, https://doi.org/10.5194/tc-6-881-2012.

Connolly, R., M. Connolly, and W. Soon, 2017: Re-calibration of Arctic sea ice extent datasets using Arctic surface air temperature records. *Hydrological Sciences Journal*, **62**, 1317–1340, https://doi.org/10.1080/02626667.2017.1324974.

Day, J. J., J. C. Hargreaves, J. D. Annan, and A. Abe-Ouchi, 2012: Sources of multi-decadal variability in Arctic sea ice extent. *Environmental Research Letters*, **7**, 034011, https://doi.org/10.1088/1748-9326/7/3/034011.

Deser, C., and H. Y. Teng, 2008: Evolution of Arctic sea ice concentration trends and the role of atmospheric circulation forcing, 1979–2007. *Geophys. Res. Lett.*, **35**, L02504, https://doi.org/10.1029/2007GL032023.

Gao, Y. Q., and Coauthors, 2015: Arctic sea ice and Eurasian climate: A review. *Adv. Atmos. Sci.*, **32**, 92–114, https://doi.org/10.1007/s00376-014-0009-6.

Harris, I., T. J. Osborn, P. Jones, and D. Lister, 2020: Version 4 of the CRU TS monthly high-resolution gridded multivariate climate dataset. *Scientific Data*, **7**, 109, https://doi.org/10.1038/s41597-020-0453-3.

Huang, B. Y., and Coauthors, 2017a: Extended reconstructed sea surface temperature, version 5 (ERSSTv5): Upgrades, validations, and intercomparisons. *J. Climate*, **30**, 8179–8205, https://doi.org/10.1175/JCLI-D-16-0836.1.

Huang, J. B., and Coauthors, 2017b: Recently amplified arctic warming has contributed to a continual global warming trend. *Nature Climate Change*, **7**, 875–879, https://doi.org/10.1038/s41558-017-0009-5.

Ivanov, V., A. Smirnov, V. Alexeev, N. V. Koldunov, I. Repina, and V. Semenov, 2018: Contribution of convection-induced heat flux to winter ice decay in the Western Nansen Basin. *J. Geophys. Res.: Oceans*, **123**, 6581–6597, https://doi.org/10.1029/2018JC013995.

Ivanova, N., O. M. Johannessen, L. T. Pedersen, and R. T. Tonboe, 2014: Retrieval of Arctic sea ice parameters by satellite passive microwave sensors: A comparison of eleven sea ice concentration algorithms. *IEEE Trans. Geosci. Remote Sens.*, **52**, 7233–7246, https://doi.org/10.1109/TGRS.2014.2310136.

Johannessen, O. M., and Coauthors, 2004: Arctic climate change: Observed and modelled temperature and sea-ice variability. *Tellus A: Dynamic Meteorology and Oceanography*, **56**, 328–341, https://doi.org/10.3402/tellusa.v56i4.14418.

Krasheninnikova, S. B., and M. A. Krasheninnikova, 2019: Causes and features of long-term variability of the ice extent

in the Barents Sea. *Led i Sneg*, **59**, 112–122. (in Russian)

Kuzmina, S. I., O. M. Johannessen, L. Bengtsson, O. G. Aniskina, and L. P. Bobylev, 2008: High northern latitude surface air temperature: Comparison of existing data and creation of a new gridded data set 1900–2000. *Tellus A: Dynamic Meteorology and Oceanography*, **60**, 289–304, https://doi.org/10.1111/j.1600-0870.2008.00303.x.

Matveeva, T. A., and V. A. Semenov, 2022: Regional features of the Arctic sea ice area changes in 2000–2019 versus 1979–1999 periods. *Atmosphere*, **13**, 1434, https://doi.org/10.3390/atmos13091434.

Meier, W. N., and Coauthors, 2014: Arctic sea ice in transformation: A review of recent observed changes and impacts on biology and human activity. *Rev. Geophys.*, **52**, 185–217, https://doi.org/10.1002/2013RG000431.

Miles, M. W., D. V. Divine, T. Furevik, E. Jansen, M. Moros, and A. E. J. Ogilvie, 2014: A signal of persistent Atlantic multidecadal variability in Arctic sea ice. *Geophys. Res. Lett.*, **41**, 463–469, https://doi.org/10.1002/2013GL058084.

Notz, D., and SIMIP Community, 2020: Arctic Sea Ice in CMIP6. *Geophys. Res. Lett.*, **47**, e2019GL086749, https://doi.org/10.1029/2019GL086749.

Pishchalnik, V. M., V. A. Romanyuk, I. G. Minervin, and A. S. Batuhtina, 2016: Analysis of dynamics for anomalies of the ice cover in the Okhotsk Sea in the period from 1882 to 2015. *Izvestiya TINRO*, **185**, 228–239. (in Russian)

Plotnikov, V. V., and N. M. Vakulskaya, 2012: Variability of ice conditions in the Bering Sea in the second half of 20 century and the beginning of 21 century. *Izvestiya TINRO*, **170**, 220–228. (in Russian)

Polyakov, I. V., and Coauthors, 2003: Long-term ice variability in Arctic marginal seas. *J. Climate*, **16**, 2078–2085, https://doi.org/10.1175/1520-0442(2003)016<2078:LIVIAM>2.0.CO;2.

Polyakov, I. V., and Coauthors, 2017: Greater role for Atlantic inflows on sea-ice loss in the Eurasian Basin of the Arctic Ocean. *Science*, **356**, 285–291, https://doi.org/10.1126/science.aai8204.

Rayner, N. A., D. E. Parker, E. B. Horton, C. K. Folland, L. V. Alexander, D. P. Rowell, E. C. Kent, and A. Kaplan, 2003: Global analyses of sea surface temperature, sea ice, and night marine air temperature since the late nineteenth century. *J. Geophys. Res.: Atmos.*, **108**, 4407, https://doi.org/10.1029/2002JD002670.

Semenov, V. A., 2014: Role of sea ice in formation of wintertime arctic temperature anomalies. *Izvestiya, Atmospheric and Oceanic Physics*, **50**, 343–349, https://doi.org/10.1134/S0001433814040215.

Semenov, V. A., and M. Latif, 2012: The early twentieth century warming and winter Arctic sea ice. *The Cryosphere*, **6**, 1231–1237, https://doi.org/10.5194/tc-6-1231-2012.

Semenov, V. A., and T. A. Matveeva, 2020: Arctic sea ice in the first half of the 20th century: Temperature-based spatiotemporal reconstruction. *Izvestiya, Atmospheric and Oceanic Physics*, **56**, 534–538, https://doi.org/10.1134/S0001433820050102.

Semenov, V. A., T. Martin, L. K. Behrens, and M. Latif, 2015: Arctic sea ice area in CMIP3 and CMIP5 climate model ensembles –variability and change. *The Cryosphere*, **9**, 1077–1131, https://doi.org/10.5194/tcd-9-1077-2015.

Semenov, V. A., M. Latif, D. Dommenget, N. S. Keenlyside, A. Strehz, T. Martin, and W. Park, 2010: The impact of North Atlantic–Arctic multidecadal variability on Northern Hemisphere surface air temperature. *J. Climate*, **23**, 5668–5677, https://doi.org/10.1175/2010JCLI3347.1.

Svendsen, L., N. Keenlyside, M. Muilwijk, I. Bethke, N. E. Omrani, and Y. Q. Gao, 2021: Pacific contribution to decadal surface temperature trends in the Arctic during the twentieth century. *Climate Dyn.*, **57**, 3223–3243, https://doi.org/10.1007/s00382-021-05868-9.

Swart, N. C., J. C. Fyfe, E. Hawkins, J. E. Kay, and A. Jahn, 2015: Influence of internal variability on Arctic sea-ice trends. *Nature Climate Change*, **5**, 86–89, https://doi.org/10.1038/nclimate2483.

Timokhov, L. A., N. A. Vyazigina, E. U. Mironov, and A. V. Yulin, 2019: Climatic changes of seasonal and inter-annual variability of the ice cover of the Greenland and Barents Seas. *Arctic and Antarctic Research*, **65**, 148–168, https://doi.org/10.30758/0555-2648-2019-65-2-148-168.

Tokinaga, H., S. P. Xie, and H. Mukougawa, 2017: Early 20th-century Arctic warming intensified by Pacific and Atlantic multidecadal variability. *Proceedings of the National Academy of Sciences of the United States of America*, **114**, 6227–6232, https://doi.org/10.1073/pnas.1615880114.

Vakulskaya, N. M., V. V. Plotnikov, and V. I. Pustoshnova, 2014: The conjugacy of ice conditions of the Bering Sea with ice conditions in the seas of East Arctic sector and the Pacific Basin. *Bulletin of the Far Eastern Branch of the Russian Academy of Sciences*, **5**, 18–24. (in Russian)

Vinje, T., 2001: Anomalies and trends of sea-ice extent and atmospheric circulation in the Nordic Seas during the period 1864–1998. *J. Climate*, **14**, 255–267, https://doi.org/10.1175/1520-0442(2001)014<0255:AATOSI>2.0.CO;2.

Walsh, J. E., and C. M. Johnson, 1979: An analysis of Arctic sea ice fluctuations, 1953–77. *J. Phys. Oceanogr.*, **9**, 580–591, https://doi.org/10.1175/1520-0485(1979)009<0580:AAOASI>2.0.CO;2.

Walsh, J. E., F. Fetterer, J. S. Stewart, and W. L. Chapman, 2017: A database for depicting Arctic sea ice variations back to 1850. *Geographical Review*, **107**, 89–107, https://doi.org/10.1111/j.1931-0846.2016.12195.x.

Wang, M. Y., and J. E. Overland, 2012: A sea ice free summer Arctic within 30 years: An update from CMIP5 models. *Geophys. Res. Lett.*, **39**, L18501, https://doi.org/10.1029/2012GL052868.

Wendler, G., and T. Wong, 2019: Recent substantial changes in Bering Sea ice cover (German). *Polarforschung*, **88**, 151–156, https://doi.org/10.2312/polarforschung.88.2.151.

Wendler, G., L. Chen, and B. Moore, 2014: Recent sea ice increase and temperature decrease in the Bering Sea area, Alaska. *Theor. Appl. Climatol.*, **117**, 393–398, https://doi.org/10.1007/s00704-013-1014-x.

Yamanouchi, T., 2011: Early 20th century warming in the Arctic: A review. *Polar Science*, **5**(1), 53–71, https://doi.org/10.1016/j.polar.2010.10.002.

Yang, X.-Y., G. H. Wang, and N. Keenlyside, 2020: The Arctic sea ice extent change connected to Pacific decadal variability. *The Cryosphere*, **14**, 693–708, https://doi.org/10.5194/tc-14-693-2020.

Zakharov, V. E. 1997: *Sea Ice in the Climate System*. World Climate Research Programme/Arctic Climate System Study, WMOITD 782, World Meteorological Organization , Geneva , 80 pp.

Zhang, J. L., R. Woodgate, and R. Moritz, 2010: Sea ice response to atmospheric and oceanic forcing in the bering sea. *J. Phys. Oceanogr.*, **40**, 1729–1747, https://doi.org/10.1175/2010JPO4323.1.

Zhang, R., 2015: Mechanisms for low-frequency variability of summer Arctic sea ice extent. *Proceedings of the National Academy of Sciences of the United States of America*, **112**, 4570–4575, https://doi.org/10.1073/pnas.1422296112.